Quantum Entropic Self-Localization with Ultracold Fermions

Mikhail Mamaev,[1,2,3,*] Itamar Kimchi,[1,2,3] Michael A. Perlin,[1,2,3] Rahul M. Nandkishore,[2,3] and Ana Maria Rey[1,2,3]
[1]JILA and NIST, University of Colorado, Boulder, Colorado 80309, USA
[2]Department of Physics, University of Colorado, Boulder, Colorado 80309, USA
[3]Center for Theory of Quantum Matter, University of Colorado, Boulder, Colorado 80309, USA

(Received 1 July 2019; published 27 September 2019)

We study a driven, spin-orbit coupled fermionic system in a lattice at the resonant regime where the drive frequency equals the Hubbard repulsion, for which nontrivial constrained dynamics emerge at fast timescales. An effective density-dependent tunneling model is derived, and it is examined in the sparse filling regime in one dimension. The system exhibits entropic self-localization, where while even numbers of atoms propagate ballistically, odd numbers form localized bound states induced by an effective attraction from a higher configurational entropy. These phenomena occur in the strong coupling limit where interactions impose only a constraint with no explicit Hamiltonian term. We show how the constrained dynamics lead to quantum few-body scars and map to an Anderson impurity model with an additional intriguing feature of nonreciprocal scattering. Connections to many-body scars and localization are also discussed.

DOI: 10.1103/PhysRevLett.123.130402

Introduction.—Ultracold atomic systems loaded into optical lattices are among the most powerful quantum simulation platforms accessible today, especially when augmented with emerging capabilities for individual-particle manipulation. Dynamical control over internal and external degrees of freedom, lack of disorder, long coherence times, and tunable interactions allow these systems to capture many of the ingredients at the heart of modern quantum science [1]. These include gauge fields [2], superconductivity [3], and even phenomena relevant to high-energy physics such as confinement [4]. However, optical lattice systems are often limited by slow effective cross-site interaction timescales such as superexchange in the Mott insulating regime.

In this Letter, we look at a resonance-assisted model operating in the strongly interacting regime. This model gives rise to constrained physics where atomic motion is strongly correlated and species dependent, while evolving at timescales set by the lattice tunneling rate. Our model employs a driving laser that interrogates internal pseudospin states, and imposes a relative phase between every lattice site which generates spin-orbit coupling (SOC) [5–8]. The competition between the SOC-inducing drive and interactions makes one tunneling process resonant and inhibits the other processes, yielding an effective density-dependent tunneling. This setup is connected to prior experiments using tilted [9–13] and shaken lattices [14–20] to study gauge fields [21–26], transport [27,28], Mott-metal transitions [29], and many other phenomena [30]. Our Letter avoids the issue of heating effects caused by Floquet engineering, has a straightforward implementation, and explores subjects of scattering and localization that have not been considered as often in this context [31,32]. This Letter is also related to the prior proposal of generating cluster states [33] but now explores the nonperturbative regime where conventional superexhange breaks down.

The density-dependent model we derive exhibits multibody self-localization, where particles localize themselves without additional external potentials. The effect is akin to a quantum entropic self-confinement, caused by the emergence of bound states induced by the minimization of kinetic energy in Fock states with higher connectivity. The bound states feature different physics than other mobile scattering states, a behavior that is reinforced by mapping the dynamics to an Anderson impurity model [34–36], allowing us to derive analytic results on bound populations and scattering coefficients. This mapping is also supplemented by a particular type of asymmetric behavior similar to those found in nonreciprocal systems [37], manifesting as a scattering process where transmission moves a scatterer while reflection keeps it in place. These constrained dynamics are connected to the study of quantum scars [38–40] as closed trajectories arise depending on the boundaries, drastically changing the longtime density profiles. Our results are also similar to those seen in Efimov physics [41–43] since our system exhibits a three-body bound state and free-propagating two-body pairs. While the physics described here is at the level of a 1D system for which a hard-core boson description would yield equivalent results, the experimental implementation poses no significant restriction on dimension. This opens a wealth of prospects for further studies of even richer phenomena in higher dimensions, where Fermi statistics

will matter and the features of quantum scars and nonreciprocity become qualitatively distinct.

The system can be realized experimentally in a number of platforms. The most promising one is 3D optical lattices using ultracold alkaline-earth atoms, for which the long lifetimes and magnetic field insensitivity permit a clean study. Having faster timescales also permits implementation in systems with access to modern tools that allow for single-atom addressability, such as quantum gas microscopes [44–49] and optical tweezers [50–53], which would facilitate easier observation of the dynamics.

Model.—Our starting point is a cubic optical lattice of L sites populated by N fermionic atoms with two internal pseudospin states g, e in the lowest Bloch band. The system is 3D in principle, although in this Letter we restrict to 1D by making the lattice confinement stronger along transverse directions. A resonant interrogating laser drives transitions between the internal states. The Hamiltonian is $\hat{H} = \hat{H}_0 + \hat{H}_\Omega$, where $\hat{H}_0/\hbar = -J\sum_{\langle i,j\rangle,\sigma}(\hat{c}^\dagger_{i,\sigma}\hat{c}_{j,\sigma} + \text{H.c.}) + U\sum_j \hat{n}_{j,e}\hat{n}_{j,g}$ is the Fermi-Hubbard model (nearest-neighbor tunneling), and $\hat{H}_\Omega/\hbar = (\Omega/2)\sum_j(-1)^j(\hat{c}^\dagger_{j,e}\hat{c}_{j,g} + \text{H.c.})$ is the laser drive. Here, $\hat{c}_{j,\sigma}$ annihilates an atom of spin $\sigma \in \{g, e\}$ on site j, and $\hat{n}_{j,\sigma} = \hat{c}^\dagger_{j,\sigma}\hat{c}_{j,\sigma}$. The lattice tunneling rate is J, and the on-site repulsion is U. The laser drive has Rabi frequency Ω and a site-dependent phase $e^{ij\pi} = (-1)^j$ arising from a mismatch between the driving and confining laser wavelengths, generating SOC [5–7]. Every adjacent pair of sites has a relative phase of π, resulting in a relative minus sign between their laser couplings. Figure 1(a) depicts the setup.

We define two new species of fermion, $\hat{a}_{j,\uparrow} = [\hat{c}_{j,e} + (-1)^j\hat{c}_{j,g}]/\sqrt{2}$ and $\hat{a}_{j,\downarrow} = [\hat{c}_{j,e} - (-1)^j\hat{c}_{j,g}]/\sqrt{2}$, for which the Hamiltonian becomes

$$\hat{H}/\hbar = -J\sum_{\langle i,j\rangle}(\hat{a}^\dagger_{i,\uparrow}\hat{a}_{j,\downarrow} + \text{H.c.}) + U\sum_j \hat{n}_{j,\uparrow}\hat{n}_{j,\downarrow} + \frac{\Omega}{2}\sum_j(\hat{n}_{j,\uparrow} - \hat{n}_{j,\downarrow}), \quad (1)$$

with number operators $\hat{n}_{j,\sigma'} = \hat{a}^\dagger_{j,\sigma'}\hat{a}_{j,\sigma'}$ for new pseudospin states $\sigma' \in \{\uparrow, \downarrow\}$. The laser drive in this frame acts as an effective magnetic field. Tunneling is accompanied by a spin flip due to the SOC. Direct tunneling into empty sites must cross an energy gap $\pm\Omega$ and is inhibited for strong driving $\Omega/J \gg 1$.

However, if we tune the drive strength to match the repulsion $U = \Omega$, an $\uparrow$ atom can tunnel into a site already holding an $\uparrow$ atom by flipping its spin and creating a doublon (two atoms of opposite spin). The energy loss $-\Omega$ is resonantly compensated for by an energy gain U from repulsion, with total cost $-\Omega + U = 0$ allowing the process to occur freely at rate J. A $\downarrow$ atom tunneling into a site with another $\downarrow$ atom would instead cost $+\Omega + U = 2U$ and would still be inhibited. Since tunneling into an already-occupied state is Pauli blocked, the process described is the only one that can occur. In the limit $U/J = \Omega/J \to \infty$, we thus reduce the Hamiltonian to a density-dependent tunneling model (up to J/U corrections),

$$\hat{H}_\infty/\hbar = -J\sum_{\langle i,j\rangle}\hat{n}_{j,\uparrow}(1 - \hat{n}_{i,\downarrow})(\hat{a}^\dagger_{j,\downarrow}\hat{a}_{i,\uparrow} + \text{H.c.}), \quad (2)$$

where the number terms ensure that the spin-flip tunneling has an $\uparrow$ atom on the destination and no $\downarrow$ atom on the origin. This model is valid for timescales $tJ \lesssim U/J$; see Sec. E of the Supplemental Material [54] for benchmarking.

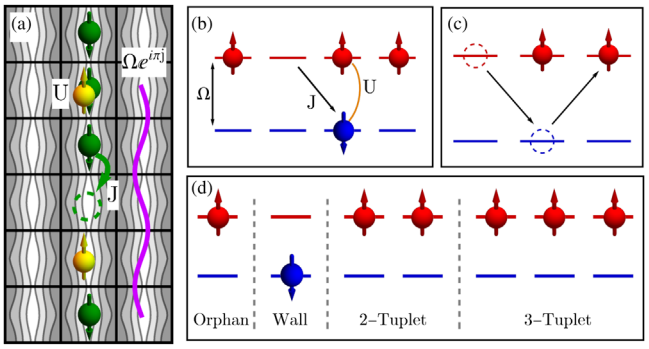

FIG. 1. (a) Schematic of Fermi-Hubbard optical lattice setup, confined to 1D, driven by a SOC-inducing laser with relative phase π between sites. (b) Resonance-assisted atomic motion in the gauged frame. An $\uparrow$ atom can tunnel into a neighboring site already holding an $\uparrow$ atom, flipping its spin, and creating a doublon. All other tunneling processes are off resonant. (c) Leapfrog motion of two $\uparrow$ atoms. (d) Few-body structures present in a sparsely filled lattice. Orphans cannot move on their own, but they interact with other atoms. Walls inhibit all motion and cannot move. A 2-tuplet moves freely via the leapfrog mechanism. A 3-tuplet can shoot off a 2-tuplet but exhibits nontrivial three-body dynamics.

The constrained motion is depicted in Fig. 1(b), and it can be understood as a leapfrog mechanism alternating between doublons and neighboring $\uparrow$ singlons (single atoms). Assuming a sparse lattice with $N/L \ll 1$, we categorize the behavior of few-atom configurations in Fig. 1(c). An $\uparrow$ singlon is an orphan which cannot move on its own but will interact with other atoms. A $\downarrow$ singlon can neither move nor permit motion through itself, acting as a wall. A 2-tuplet (two adjacent $\uparrow$ singlons) moves freely via the leapfrog mechanism. A 3-tuplet (three adjacent $\uparrow$ singlons) can also move by shooting off a 2-tuplet but exhibits nontrivial three-body dynamics that we discuss below.

In Fig. 2, we compare the density $\langle\hat{n}_j\rangle = \langle\hat{n}_{j,\uparrow}\rangle + \langle\hat{n}_{j,\downarrow}\rangle$ profiles of a 2-tuplet propagating freely [Fig. 2(a)], colliding with a wall [Fig. 2(b)], and with an orphan [Fig. 2(c)]. The 2-tuplet acts as a quasiparticle that spreads ballistically, with wave fronts rising from an underlying quantum walk.

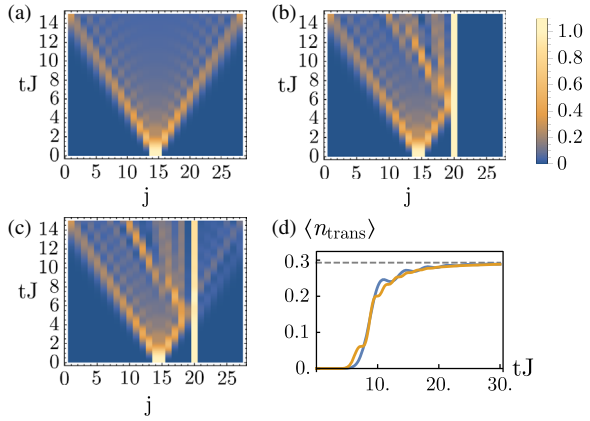

FIG. 2. (a) Dynamics of an initial 2-tuplet [using Eq. (2)]. We plot atomic density $\langle \hat{n}_j \rangle$ (color scaled to emphasize features). (b) Reflection of a propagating 2-tuplet off a wall (↓ singlon). (c) Collision of a propagating 2-tuplet with an orphan (↑ singlon). Three-body dynamics cause nonreciprocal transmission and reflection. (d) Number of atoms transmitted past the orphan during the collision in panel (c). The orange line is direct Fermi-Hubbard numerics. The blue line uses a Kronecker-delta potential single-particle scattering of strength $U_\delta = 2J$, which has an asymptotic value of $\langle \hat{n}_{\text{trans}} \rangle = 1 - 1/\sqrt{2}$ indicated in gray (see the discussion of scattering in the text).

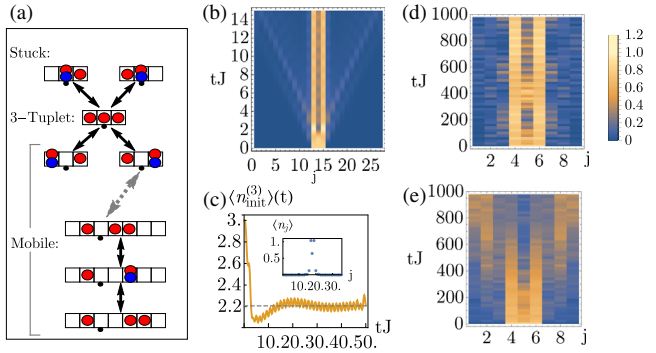

FIG. 3. (a) Schematic for a 3-tuplet's motion. Red and blue circles are ↑, ↓ atoms respectively. The 3-tuplet can tunnel into four states: two stuck states, and two mobile (scattering) states that shoot off a 2-tuplet. The dots under the boxes indicate the center of the 3-tuplet. (b) Density dynamics for an initial 3-tuplet. (c) Number of atoms that stay in the initial three sites. The gray dashed line marks the analytic prediction of $\langle \hat{n}^{(3)}_{\text{init}} \rangle \approx 2.2$ (see Sec. A of the Supplemental Material [54]). (Inset) Density profile for the 3-tuplet bound eigenstates $|\phi^{(3)}_\pm\rangle$ (equal for both). (d),(e) Density dynamics of a 3-tuplet for long times $tJ \gg 1$ (coarse grained in time), for a small lattice using (d) open and (e) periodic boundaries. The periodic boundaries eventually dissolve the localization by wrapping 2-tuplets around to pull the orphan away.

Upon colliding with the orphan, we find that a nontrivial scattering process takes place. Some atom density $\langle \hat{n}_{\text{trans}} \rangle = \sum_{j>j_0} \langle \hat{n}_j \rangle$ (j_0 the position of the orphan) is transmitted by forming a new 2-tuplet with the orphan, while some is reflected. The orphan acts as an effective scatterer whose own position is changed only if transmission occurs. The underlying reason for this outcome is tied to the self-localization properties of the three-atom system.

Bound states of a 3-tuplet.—The core dynamics for three atoms can be understood by considering a 3-tuplet. Figure 3(a) shows the states that it can tunnel into. An atom can either tunnel into the middle, yielding stuck states that cannot move farther, or out from the middle to make a 2-tuplet free to propagate. The 3-tuplet state thus has connectivity $\nu = 4$, which counts the number of Fock states that $\hat{H}$ couples it to. If we allow a 2-tuplet to propagate, an immobile orphan is generated, and the resulting state is reduced to connectivity $\nu = 2$.

This reduced connectivity lets us map the motion of the 3-tuplet to a 1D tight-binding chain with impurities. The accessible Fock states are left- and right-side 2-tuplet states, as shown in Fig. 3(a). We associate each of these states with a virtual lattice coordinate m (one for the doublon configuration, and one for neighboring singlons), with two virtual sites m for every real site j. The 3-tuplet acts as a central site coupling to the left- and right-chains of states. In addition, it also couples to the two stuck states, acting as extra dead-end links. This model is analogous to a noninteracting Anderson impurity model (see Sec. A of the Supplemental Material [54]),

$$\hat{H}^{(3)}/\hbar = -J \sum_{\langle m,n \rangle} (\hat{d}^\dagger_m \hat{d}_n + \text{H.c.}) - J(\hat{d}^\dagger_0 \hat{d}_L + \hat{d}^\dagger_0 \hat{d}_R + \text{H.c.}), \tag{3}$$

where $\hat{d}_m$ annihilates a fermion on virtual site m, $\hat{d}_0$ on the 3-tuplet, and $\hat{d}_L$, $\hat{d}_R$ on the stuck states (acting as impurities). The Anderson impurity model is known to host bound states, and indeed, we observe their presence in our system as well. Figure 3(b) shows the density dynamics for an initial 3-tuplet. In contrast to the 2-tuplet, more than 2/3 of the atoms remain at the sites that they started in; see Fig. 3(c), where $\langle \hat{n}^{(N)}_{\text{init}} \rangle$ is the total atom number summing over the N initially filled sites. The 3-tuplet has overlap with exponentially localized bound eigenstates, and the corresponding population will not decrease as the system evolves. We find two such bound eigenstates, $\hat{H}_\infty |\phi^{(3)}_\pm\rangle = \pm \hbar E |\phi^{(3)}_\pm\rangle$ (up to exponentially small boundary corrections), with energy $E = \sqrt{2} bJ$, where $b^2 = 1 + \sqrt{2}$ is the wave function localization length in units of the real lattice spacing (see Sec. A of the Supplemental Material [54] for analytic forms of the eigenstates). In the limit $L \to \infty$, the 3-tuplet $|\uparrow,\uparrow,\uparrow\rangle$ has overlap $|\langle \uparrow,\uparrow,\uparrow | \phi^{(3)}_\pm \rangle|^2 = 1/(2\sqrt{2})$ with each bound eigenstate. Each of these eigenstates has $\langle \hat{n}^{(3)}_{\text{init},\pm} \rangle = 2 + 1/\sqrt{2}$ atoms on the initially occupied sites [Fig. 3(c) inset]. We then find that a 3-tuplet should have $\langle \hat{n}^{(3)}_{\text{init}} \rangle \approx 2.2$ atoms localized in the longtime limit, which matches direct numerics in Fig. 3(c).

This self-localization shows a stark difference between open and periodic boundary conditions, as evident from the density of an initial 3-tuplet over longer timescales [Figs. 3(d) and 3(e)]. For periodic boundaries, the 3-tuplet position eventually dissolves, as a 2-tuplet can wrap around the lattice and collide with the orphan from the opposite side. If another 2-tuplet then shoots off, now involving the old orphan, the new orphan will have moved outside the initial three sites. The timescale for this dissolving process grows with system size since 2-tuplets must cross the entire lattice. For open boundaries, the 2-tuplets can only rebound off the wall and come back, allowing localization to persist. This is indicative of the presence of quantum few-body scars [62], as the system exhibits closed trajectories with reduced dimension of accessible Hilbert space size changing the longtime behavior.

The multibody self-localization shown in Fig. 3 can be interpreted as a coherent quantum version of entropic confinement, where the system tends to stay in states with higher connectivity ν to reduce its kinetic energy. This is analogous to the three-body bound states described by Efimov physics, although the system itself is quite different. While the higher energy scales in the system ($U = \Omega$) are not present in the effective Hamiltonian, they manifest indirectly by energetically enforcing restrictions on the motion. Localization is also present in higher-order N-tuplet structures (N neighboring $\uparrow$ singlons), as seen in Fig. 4. We find that even-N configurations will smear out quickly, while odd-N configurations exhibit longtime localization for similar reasons (see Sec. B of the Supplemental Material [54]).

Scattering.—We can use the intuitions developed above to understand the 2-tuplet and orphan scattering in Figs. 2(c) and 2(d). As discussed in the previous section and Sec. A of the Supplemental Material [54], the Hamiltonian for 3-tuplets can be reduced to a tight-binding chain with a single impurity state shifted in energy (though there are two stuck states, one linear combination decouples). We can further remodel the scattering as a single-particle problem, with a quasiparticle (corresponding to a 2-tuplet) moving though a Kronecker-delta potential formed by the impurity (corresponding to an orphan). Under this picture, Eq. (3) can be rewritten as $\hat{H}^{(3)}_{\mathrm{eff}}/\hbar = -J\sum_{\langle m,n\rangle}(\hat{d}^{\dagger}_m\hat{d}_n + \mathrm{H.c.}) - U_\delta\hat{d}^{\dagger}_0\hat{d}_0$ for a potential depth U_δ. We estimate the transmission by initializing a particle at $m_{\mathrm{init}} < 0$ and evaluating its density at all $m > 0$ for times $tJ \gtrsim |m_{\mathrm{init}}|$, rescaling the time and amplitude by 2 (since a 2-tuplet takes two steps to move one real lattice site, and has two atoms).

Figure 2(d) compares this estimated transmission amplitude with direct three-atom numerics. With a potential depth of $U_\delta = 2J$, corresponding to the same bound-state localization length b in the single- and three-particle problems, we find good agreement. This simplification also lets us find an analytic expression for the transmission,

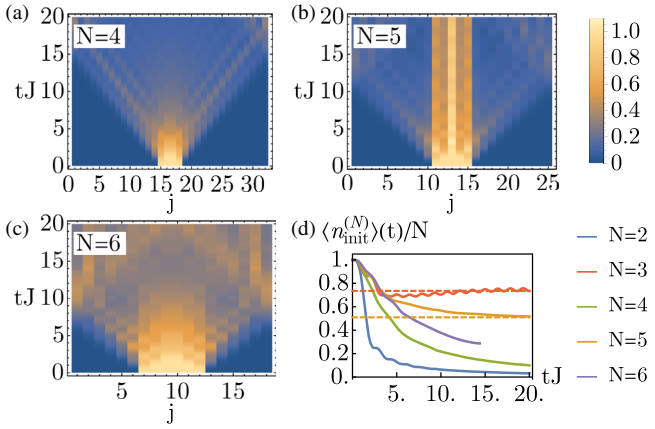

FIG. 4. Density dynamics of an N-tuplet of $\uparrow$ atoms, for (a) $N = 4$, (b) $N = 5$, and (c) $N = 6$. Localization persists for odd $N = 5$, but not the even cases. (d) Total number of remaining atoms in the initially populated sites for $N = 2, 3, 4, 5, 6$. System sizes are $L = 36, 35, 32, 25, 18$. The red dashed line is the analytic prediction for $N = 3$ (cf. Sec. A of the Supplemental Material [54]). The orange dashed line is a quasinumeric prediction from a bound-state search for $N = 5$ (see Sec. B of the Supplemental Material [54]). The even lines are expected to stabilize at mean density N/L in the longtime limit. Note that the $N = 6$ line is stopped early to avoid rebounds from the edges.

yielding $\langle\hat{n}_{\mathrm{trans}}\rangle = 1 - 1/\sqrt{2} \approx 0.29$ (see Sec. C of the Supplemental Material [54]). The agreement in Fig. 2(d) showcases the reduction of a three-body interacting problem to that of a single particle with tractable emergent interactions.

The nontrivial feature not captured by this mapping is the nonreciprocal position dependence of the scatterer. Consider an orphan initially on the right of the three sites of an imminent collision. If the 2-tuplet reflects, then the orphan remains in place. If transmission occurs, then a new 2-tuplet shoots off to the right, leaving a new orphan two sites left of the original orphan's location. The system exhibits nonreciprocal behavior where the scatterer is shifted by two sites upon transmission, but not upon reflection. In a classical description, its effective mass is infinite for reflection but finite (and set by quantized motion) for transmission. This behavior is evident in the vertical stripe of atomic density two sites left of the orphan in Fig. 2(c). Finding such nonreciprocal effects in a purely closed system as a consequence of interaction-induced constraints is an intriguing feature impossible to capture with the Anderson mapping in Eq. (3).

Experimental implementations.—Realizing this system is straightforward with a 3D optical lattice populated by two-level atoms. A suggested implementation with, e.g., ^{87}Sr is to set the confinement to $V_x \sim 8E_R$–$20E_R$, and V_y, $V_z \gtrsim 100E_R$ (with E_R being the lattice recoil energy), such that on-site repulsion satisfies $U/J \sim 30$–500 [63]. The dynamical timescale will then be set by $J \sim 10$–$100 \times 2\pi$Hz. To generate the desired SOC, one

could use an optical transition in alkaline-earth atoms, or a Raman transition in alkali atoms. In both cases, it is required that the laser-imparted phase along $\hat{x}$ is π per lattice site. A coherence time much longer than the one set by J is also required. This condition is much more favorable that the stringent condition required to observe superexchange interactions (set by J^2/U).

Measurement and preparation of the few-body atomic structures are easiest to do with quantum gas microscopes and optical tweezers, respectively. However, a state-of-the-art optical lattice clock such as the ^{87}Sr clock [64,65] can also probe the 3-tuplet localization without single-site resolution. A sparse configuration of many 3-tuplets can be generated with a lattice tilt and a pulse sequence capable of spectroscopically resolving a specific set of transitions (see Sec. D in the Supplemental Material [54]). Allowing the system to evolve and then undoing the pulse sequence to detect the percentage of the atoms remaining in the initial triply occupied sites can be used to verify localization.

Conclusions and outlook.—We have proposed a simple and intuitive system where spin-orbit coupling and interactions generate constrained dynamics. This system exhibits features of self-localization and nonreciprocity, and it maps to noninteracting models while maintaining nontrivial lattice effects. A vast number of extensions can be considered, especially if one looks to higher densities or higher dimensions. At higher densities, $\downarrow$ singlons will act as bottlenecks, generically producing many-body quantum scars. Even with no $\downarrow$ singlons, a transfer matrix calculation analogous to Ref. [66] reveals that in the thermodynamic limit, there will be an exponentially large subspace of 2^L product states which will be eigenstates of the dynamics and hence will be perfect many-body quantum scars (see Sec. F in the Supplemental Material [54]). The system is also simple to generalize to higher dimensions, needing only a SOC drive with a π phase along all allowed directions. The underlying physics can be connected to dynamical gauge fields, where atomic motion by one species is influenced by another in a nonreciprocal manner [21,24,26]. Higher filling fractions lead to long-range doublon correlations, which can be relevant to studies of superconductivity. Fermionic statistics will also play a significant role in higher dimensions and interplay with the scar and nonreciprocity features. The accessible implementation and the rich breadth of physics displayed make the proposed setup an ideal playground for future investigations.

M. M. acknowledges support from a CTQM graduate fellowship. I. K. was supported by a National Research Council Fellowship through the National Institute of Standards and Technology. R. M. N. was supported by AFOSR Grant No. FA9550-17-1-0183. A. M. R was supported by AFOSR Grant No. FA9550-18-1-0319, No. FA9550-19-1-0275 and its MURI Initiative, by DARPA and ARO Grant No. W911NF-16-1-0576, by the DARPA DRINQS grant, by ARO Single Investigator Grant No. W911NF-19-1-0210, by NSF Grants No. PHY1820885 and No. JILA-PFC PHY1734006, and by the National Institute of Standards and Technology.

*mikhail.mamaev@colorado.edu

[1] I. Bloch, J. Dalibard, and S. Nascimbene, Quantum simulations with ultracold quantum gases, Nat. Phys. **8**, 267 (2012).
[2] K. Osterloh, M. Baig, L. Santos, P. Zoller, and M. Lewenstein, Cold Atoms in Non-Abelian Gauge Potentials: From the Hofstadter "Moth" to Lattice Gauge Theory, Phys. Rev. Lett. **95**, 010403 (2005).
[3] I. Bloch, J. Dalibard, and W. Zwerger, Many-body physics with ultracold gases, Rev. Mod. Phys. **80**, 885 (2008).
[4] E. Fradkin and S. H. Shenker, Phase diagrams of lattice gauge theories with Higgs fields., Phys. Rev. D **19**, 3682 (1979).
[5] M. L. Wall, A. P. Koller, S. Li, X. Zhang, N. R. Cooper, J. Ye, and A. Maria Rey, Synthetic Spin-Orbit Coupling in an Optical Lattice Clock, Phys. Rev. Lett. **116**, 035301 (2016).
[6] S. Kolkowitz, S. L. Bromley, T. Bothwell, M. L. Wall, G. E. Marti, A. P. Koller, X. Zhang, A. M. Rey, and J. Ye, Spin-orbit-coupled fermions in an optical lattice clock, Nature (London) **542**, 66 (2017).
[7] M. Eric Tai, A. Lukin, M. Rispoli, R. Schittko, T. Menke, D. Borgnia, P. M. Preiss, F. Grusdt, A. M. Kaufman, and M. Greiner, Microscopy of the interacting Harper-Hofstadter model in the two-body limit, Nature (London) **546**, 519 (2017).
[8] S. L. Bromley, S. Kolkowitz, T. Bothwell, D. Kedar, A. Safavi-Naini, M. L. Wall, C. Salomon, A. M. Rey, and J. Ye, Dynamics of interacting fermions under spin-orbit coupling in an optical lattice clock, Nat. Phys. **14**, 399 (2018).
[9] M. Aidelsburger, M. Atala, M. Lohse, J. T. Barreiro, B. Paredes, and I. Bloch, Realization of the Hofstadter Hamiltonian with Ultracold Atoms in Optical Lattices, Phys. Rev. Lett. **111**, 185301 (2013).
[10] F. Meinert, M. J. Mark, E. Kirilov, K. Lauber, P. Weinmann, M. Gröbner, A. J. Daley, and H.-C. Nägerl, Observation of many-body dynamics in long-range tunneling after a quantum quench, Science **344**, 1259 (2014).
[11] H. Miyake, G. A. Siviloglou, C. J. Kennedy, W. C. Burton, and W. Ketterle, Realizing the Harper Hamiltonian with Laser-Assisted Tunneling in Optical Lattices, Phys. Rev. Lett. **111**, 185302 (2013).
[12] J. Simon, W. S. Bakr, R. Ma, M. Eric Tai, P. M. Preiss, and M. Greiner, Quantum simulation of antiferromagnetic spin chains in an optical lattice, Nature (London) **472**, 307 (2011).
[13] O. Jürgensen, F. Meinert, M. J. Mark, H.-C. Nägerl, and D.-S. Lühmann, Observation of Density-Induced Tunneling, Phys. Rev. Lett. **113**, 193003 (2014).
[14] H. Lignier, C. Sias, D. Ciampini, Y. Singh, A. Zenesini, O. Morsch, and E. Arimondo, Dynamical Control of Matter-Wave Tunneling in Periodic Potentials, Phys. Rev. Lett. **99**, 220403 (2007).

[15] F. Meinert, M. J. Mark, K. Lauber, A. J. Daley, and H.-C. Nägerl, Floquet Engineering of Correlated Tunneling in the Bose-Hubbard Model with Ultracold Atoms, Phys. Rev. Lett. **116**, 205301 (2016).
[16] J. Struck, C. Ölschläger, R. Le Targat, P. Soltan-Panahi, A. Eckardt, M. Lewenstein, P. Windpassinger, and K. Sengstock, Quantum simulation of frustrated classical magnetism in triangular optical lattices, Science **333**, 996 (2011).
[17] G. Jotzu, M. Messer, R. Desbuquois, M. Lebrat, T. Uehlinger, D. Greif, and T. Esslinger, Experimental realization of the topological haldane model with ultracold fermions, Nature (London) **515**, 237 (2014).
[18] L. W. Clark, B. M. Anderson, L. Feng, A. Gaj, K. Levin, and C. Chin, Observation of Density-Dependent Gauge Fields in a Bose-Einstein Condensate Based on Micromotion Control in a Shaken Two-Dimensional Lattice, Phys. Rev. Lett. **121**, 030402 (2018).
[19] M. Messer, K. Sandholzer, F. Görg, J. Minguzzi, R. Desbuquois, and T. Esslinger, Floquet Dynamics in Driven Fermi-Hubbard Systems, Phys. Rev. Lett. **121**, 233603 (2018).
[20] F. Görg, M. Messer, K. Sandholzer, G. Jotzu, R. Desbuquois, and T. Esslinger, Enhancement and sign change of magnetic correlations in a driven quantum many-body system, Nature (London) **553**, 481 (2018).
[21] D. Banerjee, M. Dalmonte, M. Müller, E. Rico, P. Stebler, U.-J. Wiese, and P. Zoller, Atomic Quantum Simulation of Dynamical Gauge Fields Coupled to Fermionic Matter: From String Breaking to Evolution after a Quench, Phys. Rev. Lett. **109**, 175302 (2012).
[22] A. Bermudez, T. Schaetz, and D. Porras, Synthetic Gauge Fields for Vibrational Excitations of Trapped Ions, Phys. Rev. Lett. **107**, 150501 (2011).
[23] P. Hauke, O. Tieleman, A. Celi, C. Ölschläger, J. Simonet, J. Struck, M. Weinberg, P. Windpassinger, K. Sengstock, M. Lewenstein *et al.*, Non-Abelian Gauge Fields and Topological Insulators in Shaken Optical Lattices, Phys. Rev. Lett. **109**, 145301 (2012).
[24] L. Barbiero, C. Schweizer, M. Aidelsburger, E. Demler, N. Goldman, and F. Grusdt, Coupling ultracold matter to dynamical gauge fields in optical lattices: From flux-attachment to Z_2 lattice gauge theories, arXiv:1810.02777.
[25] F. Görg, K. Sandholzer, J. Minguzzi, R. Desbuquois, M. Messer, and T. Esslinger, Realisation of density-dependent Peierls phases to couple dynamical gauge fields to matter, arXiv:1812.05895 [Nat. Phys. (to be published)].
[26] C. Schweizer, F. Grusdt, M. Berngruber, L. Barbiero, E. Demler, N. Goldman, I. Bloch, and M. Aidelsburger, Floquet approach to $\mathbb{Z}_2$ lattice gauge theories with ultracold atoms in optical lattices, arXiv:1901.07103.
[27] C. P. Rubbo, S. R. Manmana, B. M. Peden, M. J. Holland, and A. Maria Rey, Resonantly enhanced tunneling and transport of ultracold atoms on tilted optical lattices, Phys. Rev. A **84**, 033638 (2011).
[28] V. V. Ivanov, A. Alberti, M. Schioppo, G. Ferrari, M. L. C. M. Artoni, M. L. Chiofalo, and G. M. Tino, Coherent Delocalization of Atomic Wave Packets in Driven Lattice Potentials, Phys. Rev. Lett. **100**, 043602 (2008).
[29] A. Zenesini, H. Lignier, D. Ciampini, O. Morsch, and E. Arimondo, Coherent Control of Dressed Matter Waves, Phys. Rev. Lett. **102**, 100403 (2009).
[30] A. Eckardt, Colloquium: Atomic quantum gases in periodically driven optical lattices, Rev. Mod. Phys. **89**, 011004 (2017).
[31] P. M. Preiss, R. Ma, M. Eric Tai, A. Lukin, M. Rispoli, P. Zupancic, Y. Lahini, R. Islam, and M. Greiner, Strongly correlated quantum walks in optical lattices, Science **347**, 1229 (2015).
[32] A. Lerose, B. Žunkovič, A. Silva, and A. Gambassi, Quasilocalized excitations induced by long-range interactions in translationally invariant quantum spin chains., Phys. Rev. B **99**, 121112(R) (2019).
[33] M. Mamaev, R. Blatt, J. Ye, and A. M. Rey, Cluster State Generation with Spin-Orbit Coupled Fermionic Atoms in Optical Lattices, Phys. Rev. Lett. **122**, 160402 (2019).
[34] P. W. Anderson, Localized magnetic states in metals, Phys. Rev. **124**, 41 (1961).
[35] A. C. Hewson, *The Kondo Problem to Heavy Fermions*, Vol. 2 (Cambridge University Press, Cambridge, England, 1997).
[36] S. K. Kehrein and A. Mielke, Theory of the anderson impurity model: The Schrieffer–Wolff transformation reexamined, Ann. Phys. (N.Y.) **252**, 1 (1996).
[37] L. Deák and T. Fülöp, Reciprocity in quantum, electromagnetic and other wave scattering, Ann. Phys. (Amsterdam) **327**, 1050 (2012).
[38] N. Shiraishi and T. Mori, Systematic Construction of Counterexamples to the Eigenstate Thermalization Hypothesis, Phys. Rev. Lett. **119**, 030601 (2017).
[39] S. Moudgalya, S. Rachel, B. A. Bernevig, and N. Regnault, Exact excited states of nonintegrable models, Phys. Rev. B **98**, 235155 (2018).
[40] C. J. Turner, A. A. Michailidis, D. A. Abanin, M. Serbyn, and Z. Papic, Weak ergodicity breaking from quantum many-body scars, Nat. Phys. **14**, 745 (2018).
[41] V. Efimov, Energy levels arising from resonant two-body forces in a three-body system, Phys. Lett. **33B**, 563 (1970).
[42] P. Naidon and S. Endo, Efimov physics: A review, Rep. Prog. Phys. **80**, 056001 (2017).
[43] Z.-Y. Shi, X. Cui, and H. Zhai, Universal Trimers Induced by Spin-Orbit Coupling in Ultracold Fermi Gases, Phys. Rev. Lett. **112**, 013201 (2014).
[44] T. Gericke, P. Würtz, D. Reitz, T. Langen, and H. Ott, High-resolution scanning electron microscopy of an ultracold quantum gas, Nat. Phys. **4**, 949 (2008).
[45] W. S. Bakr, J. I. Gillen, A. Peng, S. Fölling, and M. Greiner, A quantum gas microscope for detecting single atoms in a Hubbard-regime optical lattice, Nature (London) **462**, 74 (2009).
[46] J. F. Sherson, C. Weitenberg, M. Endres, M. Cheneau, I. Bloch, and S. Kuhr, Single-atom-resolved fluorescence imaging of an atomic mott insulator, Nature (London) **467**, 68 (2010).
[47] L. W. Cheuk, M. A. Nichols, M. Okan, T. Gersdorf, V. V. Ramasesh, W. S. Bakr, T. Lompe, and M. W. Zwierlein, Quantum-Gas Microscope for Fermionic Atoms, Phys. Rev. Lett. **114**, 193001 (2015).

[48] R. Yamamoto, J. Kobayashi, T. Kuno, K. Kato, and Y. Takahashi, An ytterbium quantum gas microscope with narrow-line laser cooling, New J. Phys. **18**, 023016 (2016).
[49] D. Mitra, P. T. Brown, E. Guardado-Sanchez, S. S. Kondov, T. Devakul, D. A. Huse, P. Schauss, and W. S. Bakr, Quantum gas microscopy of an attractive Fermi-Hubbard system, Nat. Phys. **14**, 173 (2018).
[50] M. Endres, H. Bernien, A. Keesling, H. Levine, E. R. Anschuetz, A. Krajenbrink, C. Senko, V. Vuletic, M. Greiner, and M. D. Lukin, Atom-by-atom assembly of defect-free one-dimensional cold atom arrays, Science **354**, 1024 (2016).
[51] M. A. Norcia, A. W. Young, and A. M. Kaufman, Microscopic Control and Detection of Ultracold Strontium in Optical-Tweezer Arrays, Phys. Rev. X **8**, 041054 (2018).
[52] A. Cooper, J. P. Covey, I. S. Madjarov, S. G. Porsev, M. S. Safronova, and M. Endres, Alkaline-Earth Atoms in Optical Tweezers, Phys. Rev. X **8**, 041055 (2018).
[53] S. Saskin, J. T. Wilson, B. Grinkemeyer, and J. D. Thompson, Narrow-Line Cooling and Imaging of Ytterbium Atoms in an Optical Tweezer Array, Phys. Rev. Lett. **122**, 143002 (2019).
[54] See Supplemental Material at http://link.aps.org/supplemental/10.1103/PhysRevLett.123.130402, which includes Refs. [55–61], for details on model benchmarking and mappings, scattering calculations and experimental preparation.
[55] E. N. Economou, *Green's Functions in Quantum Physics*, Vol. 3 (Springer, New York, 1983).
[56] J. Ye, H. J. Kimble, and H. Katori, Quantum State Engineering and Precision Metrology Using State-Insensitive Light Traps, Science **320**, 1734 (2008).
[57] A. Goban, R. B. Hutson, G. E. Marti, S. L. Campbell, M. A. Perlin, P. S. Julienne, J. P. D'Incao, A. M. Rey, and J. Ye, Emergence of multi-body interactions in a fermionic lattice clock, Nature (London) **563**, 369 (2018).
[58] M. M. Boyd, High precision spectroscopy of strontium in an optical lattice: Towards a new standard for frequency and time, Ph.D. thesis, University of Colorado at Boulder, 2007.
[59] M. A. Perlin and A. M. Rey, Effective multi-body SU(N)-symmetric interactions of ultracold fermionic atoms on a 3D lattice, New J. Phys. **21**, 043039 (2019).
[60] T. C. Li, H. Kelkar, D. Medellin, and M. G. Raizen, Real-time control of the periodicity of a standing wave: An optical accordion, Opt. Express **16**, 5465 (2008).
[61] S. Al-Assam, R. A. Williams, and C. J. Foot, Ultracold atoms in an optical lattice with dynamically variable periodicity, Phys. Rev. A **82**, 021604(R) (2010).
[62] E. J. Heller, Bound-State Eigenfunctions of Classically Chaotic Hamiltonian Systems: Scars of Periodic Orbits, Phys. Rev. Lett. **53**, 1515 (1984).
[63] X. Zhang, M. Bishof, S. L. Bromley, C. V. Kraus, M. S. Safronova, P. Zoller, A. M. Rey, and J. Ye, Spectroscopic observation of SU(N)-symmetric interactions in Sr orbital magnetism, Science **345**, 1467 (2014).
[64] S. L. Campbell, R. B. Hutson, G. E. Marti, A. Goban, N. Darkwah Oppong, R. L. McNally, L. Sonderhouse, J. M. Robinson, W. Zhang, B. J. Bloom *et al.*, A Fermi-degenerate three-dimensional optical lattice clock, Science **358**, 90 (2017).
[65] M. L. Wall, A. P. Koller, S. Li, X. Zhang, N. R. Cooper, J. Ye, and A. M. Rey, Synthetic Spin-Orbit Coupling in an Optical Lattice Clock, Phys. Rev. Lett. **116**, 035301 (2016).
[66] V. Khemani and R. Nandkishore, Local constraints can globally shatter Hilbert space: A new route to quantum information protection, arXiv:1904.04815.